

PARTICLE SIZE AND CONCENTRATION EFFECTS ON LOW ENERGY X-RAY ATTENUATION IN NANOSTRUCTURE AND MICROSTRUCTURE MATERIALS

by

Samira SARSHOUGH^{1,2}, **Kamal HADAD**^{1,2,3*}, and **Reza FAGHIHI**^{1,2}

¹Department of Nuclear Engineering, Shiraz University, Shiraz, Iran

²Shiraz University Radiation Research Center, Shiraz, Iran

³Shiraz University Safety Research Center, Shiraz, Iran

Scientific paper

<http://doi.org/10.2298/NTRP1801075S>

The effects of microsize and nanosize particles in composite structures as well as the incident radiation energy on X-ray attenuation is the focus of this study. To examine these effects, composite samples with different particle sizes of Al_2O_3 and with different thicknesses were prepared. Characteristic X-rays are applied as monochromatic X-rays and measurements were performed using an X-ray tube with a secondary excitation source instead of radioisotopes. In order to improve the efficiency and minimize the background effects a special detection system was designed and prepared. The linear attenuation coefficients of these samples are measured for X-ray photo energies of 6.40-28.49 keV. The results show that these low energy X-ray beams are more attenuated by nano-structured material compared to the micro-structured one.

Key words: linear attenuation coefficient, characteristic X-ray, nanostructure, microstructure

INTRODUCTION

Nanostructured materials whose structural elements have dimensions of 1-100 nm [1] are composed of nano-size grains, which consist of many atoms [2] whereas bulk materials are formed by grains in the range of tens of microns to one or more millimeters [3]. There have been many efforts to investigate the grain size effect on low energy gamma and X-ray attenuation [4-6]. It is believed that the X-ray attenuation capability of a material can be improved by adding nanosized particles compared to micro-sized particles because of their more uniform dispersion [3] also nanostructured material is more effective in attenuation of lower X-ray beam energies and there is no significant variation in X-ray attenuation at higher X-ray beam energies [7, 8].

Recently synthesis of nanosized filler-reinforced polymers has gained increasing attention for radiation shielding to produce a free lead protection device [9-10] because of their unique properties such as being more light weight. Also the effect of nanoparticle size on the dose enhancement in radiotherapy [11] and using them as contrast agents for computed tomography (CT) imaging applications [12-14] have been studied widely. It has been found that there is a significant difference between nanostructured and microstructured material in

X-ray absorption and attenuation at lower X-ray beam energies [3, 7]. In this case, the exact study of the effect of the particle size on the radiation absorption and attenuation is necessary which can supply information about the advantages of the use of nanomaterials in shielding, imaging and therapeutics.

In this study the size effect of Al_2O_3 on X-ray attenuation is investigated because of its several applications in a low energy X-ray beam. Using the semiconductor detector HpGe the linear attenuation coefficients of an epoxy resin composite in which nano- Al_2O_3 and micro- Al_2O_3 have been added in the same proportion is measured.

In order to conduct a thorough experimental study of linear attenuation coefficients at low photon energies, instead of radioisotopes, an X-ray tube with a secondary target system is employed as the excitation source. This system has the advantages of providing a relatively high flux, a wide variety of secondary target materials resulting in various photon energies, high spectral purity and easy handling [15, 16].

MATERIALS AND METHODS

Characteristic X-ray generation

To investigate the effect of particle size and X-ray energy on the linear attenuation coefficient, a mono-

* Corresponding author; e-mail: hadadk@shirazu.ac.ir

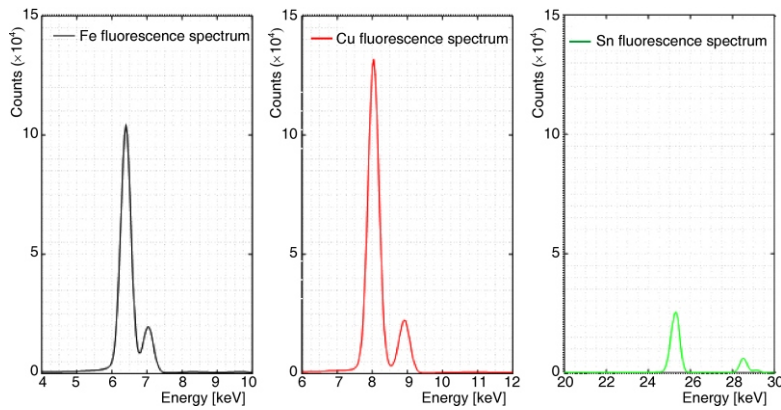


Figure 1. Fluorescence spectra of Fe, Cu, and Sn recorded by the HpGe spectrometer

chromatic X-ray beam is necessary. In this study, an X-ray tube with a secondary target system is applied as the excitation source. The X-ray tube has a tungsten anode whose maximum voltage and current are 160 kV and 20 mA, respectively. Secondary targets of Fe, Cu, and Sn are pure metals. The secondary radiations from these targets provide the incident photon energies of 6.40, 7.06, 8.05, 8.90, 25.27, and 28.49 keV. A filter whose K-edge is between K_{α} and K_{β} energies of the secondary target could be used to suppress K_{β} X-rays. Since in this study both K_{α} and K_{β} photo peaks are used as a monochromatic X-ray, this filter is not applicable to the experimental setup. In fig. 1 the fluorescence spectra of Fe, Cu, and Sn recorded by this spectrometer are shown. Full widths at half maximums (FWHM) of these photo peaks in spectra are 0.35, 0.37, 0.36, 0.38, 0.49, and 0.42 keV, respectively.

Samples fabrication

Aluminum has several applications in a low energy X-ray beam. It is widely used as an X-ray filter to attenuate low energy X-rays and hardening X-ray beam. In X-ray astronomy in order to reduce the background of the detectors several shielding materials such as aluminum oxide and aluminum nitride are used. This is due to the fact that low-Z shielding materials, at low energies, produce Auger electrons rather than fluorescent X-rays.

To prepare nanocomposite and microcomposite samples, an epoxy resin (M506) based on the bisphenol-A and hardener (HA11) polyamine was used as the polymer matrix. It is a known fact that the nanoparticles (NP) are dispersed well in the epoxy resin compared with other polymer resins. Al_2O_3 in micro-sized ($\sim 10 \mu m$) and nanosized ($\sim 10 nm$) particles supplied by Sigma-Aldrich and TECNAN companies were used to investigate the X-ray transmission through these materials. Epoxy-alumina nanocomposites and microcomposites with different contents of Al_2O_3 (*i. e.*, 4.5-9 wt. %) were fabricated through the solution casting method. The Al_2O_3 NP was agitated using an ultrasonic instrument under 100 W in acetone for 30 min. Consequently, the epoxy resin was added to the solution and

sonicated under the above condition for 30 min. The mixture was heated by a magnetic stirrer at 70 °C for 4 h to remove the acetone. Afterwards, the hardener was added and mixed by a magnetic stirrer. This mixture was degassed in a vacuum chamber and was then cast in a 4 cm \times 4 cm rectangular Lucite samples mold with a thickness of 3, 5, and 10 mm and was allowed to set over night at room temperature. Because of sedimentation of microsized particles in the epoxy resin, a new approach was applied to produce microcomposites. Microsized powder was agitated using a stirring machine at a constant speed for 15 min to ensure uniform dispersion of the powder in the epoxy matrix. Then, the hardener was added and mixed by a magnetic stirrer and cast in Lucite samples molds. This epoxy mixture in Lucite molds was degassed in a vacuum chamber. Then the upper part of the Lucite mold was barred and rotated during the curing time of the composites.

X-ray transmission measurements

The experimental arrangement used in this study is shown in fig. 2. To achieve accurate and precise results this geometrical arrangement is suggested when both the source and the detector are equipped with collimators. In this case the intensity measured by the detector will depend very sensitively on the exact geometry of the experimental system and the background effects on the spectrum transmitting through the sample are reduced considerably.



Figure 2. Set-up employed for the present measurements; 1 – collimator of the X-ray tube, 2 – secondary target, 3 – conical collimator, 4 – sample, 5 – detector collimator, 6 – vacuum pump

The transmitted spectra from nanocomposite and microcomposite samples are recorded using an HpGe detector (FWHM of 306 eV at 5.96 keV and 545 eV at 122 keV) coupled to a 2048 computerized multichannel analyzer. The detector has been calibrated using a characteristic X-ray, the energy is calculated using the following relation

$$E = a + bCh + cCh^2 \quad (1)$$

where Ch is the channel number. The centroid of the peak is calculated by the local maximum method and the width of the peak integration is set to two times the FWHM to integrate 95 % of the events counted in the peak and to minimize errors caused by misalignment of the integration window relative to the centroid of the peak [17].

Because of the high resolution of this HpGe detector in the energy range of interest, and using the area under the photo peaks to calculate linear attenuation coefficients, the effects of Compton scattering are minimized to desirable levels.

The incident (I_0) and transmitted intensities (I) are measured for a fixed preset time in each sample by determination of the center of the peak and the area under the photopeak. From the values of I , I_0 and thickness of the sample (x), the linear attenuation coefficients are obtained by using the Lambert-Beer equation

$$I = I_0 \exp(-\mu x) \quad (2)$$

The maximum uncertainty of this coefficient is calculated from uncertainties in intensities I_0 (without sample), I (with the sample) and thicknesses using the following relationship

$$(\Delta\mu) = \frac{1}{x} \frac{\Delta I_0}{I_0} + \frac{\Delta I}{I} + \frac{\Delta x}{x} \ln \frac{I_0}{I} \quad (3)$$

Since in X-ray spectrometry counting statistics normally controls the uncertainty in determining the net peak area as I or I_0 , Poisson Statistics is applied to determine the uncertainties of I or I_0 .

Thorough analysis of the problems associated with the measurements of X-ray attenuation coefficients is presented by Creagh and Hubbell [18-20]. Meanwhile, based on Creagh and Hubbell criteria in these measurements, thicknesses that satisfy -2

$\ln(I_0/I) \leq 4$ corresponds to the transmission range of 0.02 $T \leq 0.13$ and yield the best results. In this study, between three different thicknesses of nanosized and microsized composite samples, the most suitable thickness for each photo peak energy is selected to follow the mentioned criteria.

To verify our experimental arrangement, the linear attenuation coefficient of aluminum with thicknesses of 1 and 2 mm is measured and compared with theoretical values obtained by XCOM [21]. Then, the measurements are performed two times for each composite sample.

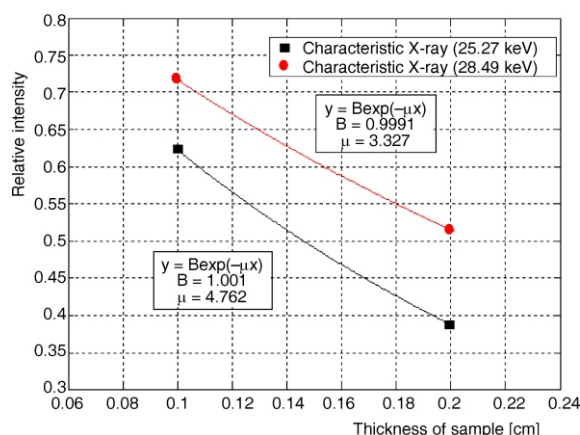


Figure 3. Relative intensity (I/I_0) of the X-ray beam at 25.27 and 28.49 keV energy variations with aluminum thickness

RESULTS AND DISCUSSION

Figure 3 shows the relative intensity (I/I_0) of the X-ray beam at 25.27 and 28.49 keV energy as a function of aluminum thickness (x). The linear attenuation coefficient is calculated by fitting equation eq. 2 to these data. As seen in this figure, the value of B is very close to unity and this indicates the establishment of a good geometry condition in this measurement (reference).

The experimental and theoretical values of the linear attenuation coefficient of aluminum are listed in tab. 1. Good agreements between them are observed and it has been concluded that our experimental arrangement is suitable for measuring the linear attenuation coefficient.

After ensuring the establishment of a good geometry condition in this measurement, the linear attenuation coefficient of the composite samples is determined. Subsequent to the fabrication of nanosized and microsized composite samples in three ranges of thickness, they are exposed to monoenergetic characteristic X-rays and linear attenuation coefficients of these samples are measured for characteristic X-ray photo energies of 6.40, 7.06, 8.05, 8.90, 25.27, and 28.49 keV belonging to Fe, Cu and Sn elements.

In fig. 4, the variations of the linear attenuation coefficient for pure epoxy and epoxy-alumina (nanosized and microsized composites) with energy for different weight fractions of Al_2O_3 are shown.

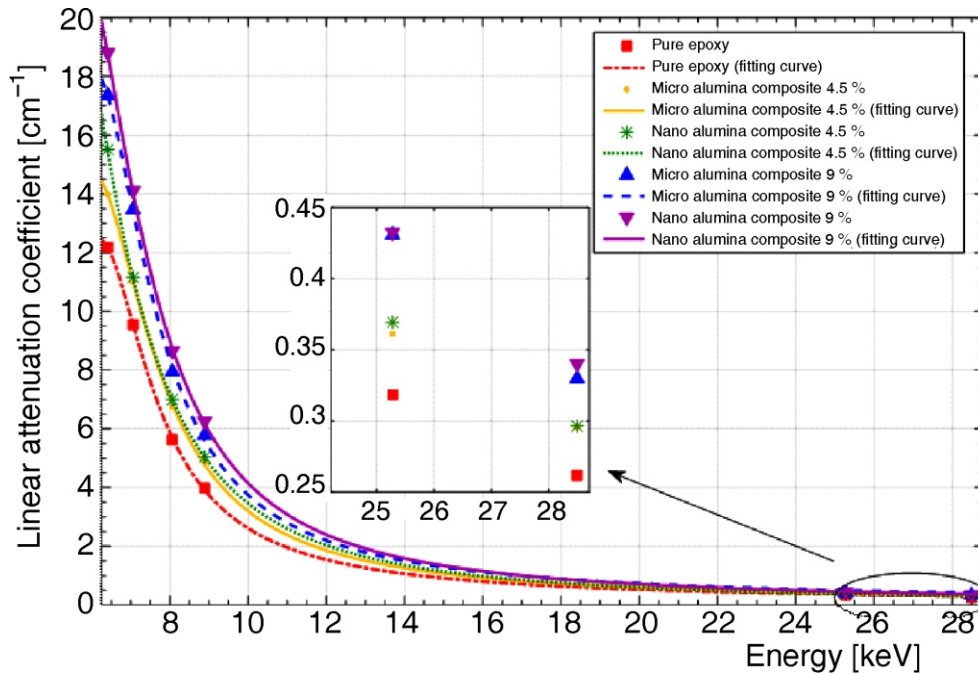
As shown in fig. 4, the X-ray linear attenuation coefficient through composite samples drops exponentially with the X-ray energy increase. Also, fig. 4

Table 1. Comparison of experimental and theoretical values of the linear attenuation coefficient of aluminum

Energy [keV]	$\mu_{Exp} [cm^{-1}]$	$\mu_{Theo} [cm^{-1}]$
25.27	4.762	4.7600
28.49	3.327	3.4607

Table 2. Linear attenuation coefficient of the pure epoxy and epoxy-alumina nanocomposites and microcomposites

Sample	Linear attenuation coefficient [cm^{-1}]											
	6.40 keV		7.06 keV		8.05 keV		8.90 keV		25.27 keV		28.49 keV	
Epoxy	12.043	0.046	9.621	0.060	5.632	0.015	3.991	0.021	0.318	0.004	0.262	0.006
Micro alumina composite 4.5 %	13.545	0.053	10.683	0.067	6.758	0.019	4.857	0.025	0.362	0.004	0.295	0.006
Nano alumina composite 4.5%	15.257	0.061	10.715	0.067	6.981	0.020	5.048	0.026	0.370	0.004	0.296	0.009
Micro alumina composite 9 %	17.457	0.075	13.400	0.089	7.947	0.023	5.774	0.029	0.431	0.004	0.330	0.006
Nano alumina composite 9 %	18.402	0.081	14.131	0.095	8.649	0.026	6.260	0.032	0.433	0.005	0.340	0.010

**Figure 4. Average relative intensity as the X-ray energy for pure epoxy and epoxy-alumina nanocomposites and microcomposites with different contents of Al_2O_3**

shows a significant difference in X-ray transmission between pure epoxy, microsized and nanosized Al_2O_3 -epoxy composites. As seen in this figure, the difference is larger at X-ray energies of 6-9 keV and drops as the X-ray energy is increased due to the particle size effect. With an increase of the nano filler (Al_2O_3) weight fraction in the composite, agglomeration causes a decrease in the nano filler effect that is clearly seen in fig. 4. Due to this phenomenon, the difference between X-ray transmission through microsized and nanosized Al_2O_3 -epoxy composites is more significant when the Al_2O_3 filler weight fraction is 4.5 % compared to 9 %.

In this study, nanosized and microsized composite samples having the most suitable thickness that satisfy the Creagh and Hubbell criteria ($2 \ln(I_0/I) < 4$) are considered to obtain the linear attenuation coefficient. The linear attenuation coefficient of these samples and its maximum deviations are shown in tab. 2.

As seen in tab. 2, the linear attenuation coefficient decreases rapidly when the X-ray photo energy increases. The linear attenuation coefficient of the nanocomposite is higher than the microcomposite in both 4.5 and 9 weight percentages because of the particle size effect.

CONCLUSIONS

In this study the effects of particle size and X-ray energy on the linear attenuation coefficient of microsized and nanosized composite materials are investigated. The linear attenuation coefficients of 3 pure epoxy, 6 nanocomposite and 6 microcomposite samples are measured for X-ray photo energies ranging from 6.40 to 28.49 keV. The results could be summarized as follows.

- As illustrated in tab. 2, the nanocomposite samples have a higher potential in attenuating X-ray photons compared to microcomposite samples. For instance, the highest difference in the linear attenuation coefficient is 13 % in the 4.5 % weight fraction samples.
- For composites with similar filler weight fractions, the difference between nanocomposites and microcomposites attenuation becomes more evident as the X-ray energy decreases in the energy range of 6.40 to 25.27 keV. The highest difference is 13% in 6.4 keV for 4.5 % weight fraction samples. There is no meaningful difference between attenuation coefficients of 9 % nanocomposites and microcomposites in 28.49 keV.

- The difference between nanocomposites and microcomposites decreases with an increase of the filler weight fraction because of the nanoparticles agglomeration phenomenon. For example, the difference in the linear attenuation coefficient is 13 % in the 4.5 % weight fraction compared to 5 % in the 9 % weight fraction at 6.4 keV.

ACKNOWLEDGMENTS

The authors are thankful to the staff of the Radiation Research Center (RRC) at Shiraz University for their assistance in the experimental setup and x-ray operation.

AUTHORS' CONTRIBUTIONS

K. Hadad devised the project and its main conceptual idea. S. Sarshough performed the experiments, calculations and analysis. K. Hadad and R. Faghihi assisted in planning and supervision of the experiments performed. S. Sarshough drafted the manuscript and K. Hadad and R. Faghihi were involved the critical revision of the paper. K. Hadad and R. Faghihi assisted in analyzing data and supervised the developments presented in this paper.

REFERENCES

[1] Moriarty, P., Nanostructured Materials, *Reports on Progress in Physics*, 64 (2001), 3, pp. 297-381

[2] Lines, M. G., Nanomaterials for Practical Functional Uses, *Journal of Alloys and Compounds*, 449 (2008), 1, pp. 242-245

[3] Botelho, M. Z., *et al.*, X-Ray Transmission through Nanostructured and Microstructured CuO Materials, *Applied Radiation and Isotopes*, 69 (2011), 2, pp. 527-530

[4] Azman, N. N., *et al.*, Characterisation of Micro-Sized and Nano-Sized Tungsten Oxide-Epoxy Composites for Radiation Shielding of Diagnostic X-Rays, *Materials Science and Engineering: C*, 33 (2013), 8, pp. 4952-4957

[5] Van den Heuvel, F., *et al.*, Beam Energy Considerations for Gold Nano-Particle Enhanced Radiation Treatment, *Physics in Medicine and Biology*, 55 (2010), 16, pp. 4509-4520

[6] Jackson, P., *et al.*, Evaluation of the Effects of Gold Nanoparticle Shape and Size on Contrast Enhancement in Radiological Imaging, *Australasian Physical & Engineering Sciences in Medicine*, 34 (2011), 2, pp. 243-249

[7] Kunzel, R., Okuno, E., Effects of the Particle Sizes and Concentrations on the X-Ray Absorption by CuO Compounds, *Applied Radiation and Isotopes*, 70 (2012), 4, pp. 781-784

[8] Azman, N. N., *et al.*, Effect of Particle Size, Filler Loadings and X-Ray Tube Voltage on the Transmitted X-Ray Transmission in Tungsten Oxide-Epoxy Com-

posites, *Applied Radiation and Isotopes*, 71 (2013), 1, pp. 62-67

[9] Haber, E. F., Froyer, G., Transparent Polymers Embedding Nanoparticles for X-Rays Attenuation, *Journal of the University of Chemical Technology and Metallurgy*, 43 (2008), 3, pp. 283-290

[10] Faccini, M., *et al.*, Development of Protective Clothing Against Nanoparticle Based on Electrospun Nanofibers, *Journal of Nanomaterials*, 2012 (2012), pp. 18-25

[11] Leung, M. K., *et al.*, Irradiation of Gold Nanoparticles by X-Rays: Monte Carlo Simulation of Dose Enhancements and the Spatial Properties of the Secondary Electrons Production, *Medical Physics*, 38 (2011), 2, pp. 624-631

[12] Xu, C., *et al.*, Size and Concentration Effect of Gold Nanoparticles on X-Ray Attenuation as Measured on Computed Tomography, *Chemistry of Materials: a Publication of the American Chemical Society*, 20 (2008), 13, pp. 4167-4169

[13] Kim, D., *et al.*, Antibiofouling Polymer-Coated Gold Nanoparticles as a Contrast Agent for In Vivo X-Ray Computed Tomography Imaging, *Journal of the American Chemical Society*, 129 (2007), 24, pp. 7661-7665

[14] Hainfeld, J. F., *et al.*, Gold Nanoparticles: a New X-Ray Contrast Agent. *The British Journal of Radiology*, 79 (2006), 939, pp. 248-253

[15] Rao, D. V., *et al.*, A New Method to Estimate Elastic Scattering Cross Sections in the X-Ray Region and the Associated Anomalous Dispersion, *Applied Radiation and Isotopes*, 49 (1998), 7, pp. 835-844

[16] Rao, D. V., *et al.*, Elastic and Compton Scattering Cross Sections in the Atomic Region $12 < Z < 82$, *Applied Radiation and Isotopes*, 47 (1996), 2, pp. 219-227

[17] Gedcke, D. A., How Counting Statistics Controls Detection Limits and Peak Precision, ORTEC Application Note AN59, 2001

[18] Creagh, D. C., Hubbell, J. H., Problems Associated with the Measurement of X-Ray Attenuation Coefficients, I. Silicon, Report of the International Union of Crystallography X-ray Attenuation Project, *Acta Crystallographica Section A: Foundations of Crystallography*, 43 (1987), 1, pp. 102-11

[19] Creagh, D. C., The Resolution of Discrepancies in Tables of Photon Attenuation Coefficients, *Nuclear Instruments and Methods in Physics Research Section A: Accelerators, Spectrometers, Detectors and Associated Equipment*, 255 (1987), 1-2, pp. 1-16

[20] Singh, K., *et al.*, Gamma-Ray Attenuation Coefficients in Bismuth Borate Glasses, *Nuclear Instruments and Methods in Physics Research Section B: Beam Interactions with Materials and Atoms*, 194 (2002), 1, pp. 1-6

[21] Berger, M., *et al.*, XCOM: Photon Cross Section Database (Version 3.1), National Institute of Standards and Technology, Gaithersburg, Md., USA, 2010, [Online] <http://physics.nist.gov/xcom>.

Received on October 8, 2107

Accepted on February 7, 2018

Самира САРШОУГ, Камал ХАДАД, Реза ФАЦИХИ

**УТИЦАЈ КОНЦЕНТРАЦИЈЕ И ВЕЛИЧИНЕ ЧЕСТИЦА НА СЛАБЉЕЊЕ
НИСКОЕНЕРГЕТСКОГ Х-ЗРАЧЕЊА У НАНОСТРУКТУРНИМ И
МИКРОСТРУКТУРНИМ МАТЕРИЈАЛИМА**

Предмет истраживања у раду су утицаји микрочестица и наночестица у композитним структурама, као и деловање упадне енергије зрачења, на слабљење Х-зрачења. Како би се испитали ови утицаји направљени су композитни узорци различитих дебљина са различитим величинама честица Al_2O_3 . Карактеристично Х-зрачење је примењено у виду монохроматског Х-зрачења и мерења су извршена применом рендгенске цеви као извора секундарне ексцитације уместо радиоизотопа. Да би се побољшала ефикасност детекције и минимизовао утицај позадине, развијен је посебан детекторски систем. Измерен је линеарни коефицијент слабљења припремљених узорака за енергије Х-зрачења од 6.4 keV до 28.49 keV. Резултати показују да је слабљење нискоенергетског Х-зрачења у наноструктурним материјалима интензивније него у микроструктурним материјалима.

Кључне речи: линеарни коефицијент слабљења, карактеристично Х-зрачење, наноструктура, микроструктура
